

# Label Mask AutoEncoder(L-MAE): A Pure Transformer Method to Augment Semantic Segmentation Datasets

Jiaru Jia<sup>1</sup>, Mingzhe Liu<sup>1</sup>, Jiake Xie<sup>2</sup>, Xin Chen<sup>1</sup>, Aiqing Yang<sup>1</sup>, Xin Jiang<sup>1</sup>, Hong Zhang<sup>1</sup>, and Yong Tang<sup>2</sup>

<sup>1</sup>Chengdu University of Technology <sup>2</sup>Picup.ai

jjrccop@gmail.com

## Abstract

*Semantic segmentation models based on the conventional neural network can achieve remarkable performance in such tasks, while the dataset is crucial to the training model process. Significant progress in expanding datasets has been made in semi-supervised semantic segmentation recently. However, completing the pixel-level information remains challenging due to possible missing in a label. Inspired by Mask AutoEncoder, we present a simple yet effective Pixel-Level completion method, **Label Mask AutoEncoder(L-MAE)**, that fully uses the existing information in the label to predict results. The proposed model adopts the fusion strategy that stacks the label and the corresponding image, namely **Fuse Map**. Moreover, since some of the image information is lost when masking the **Fuse Map**, direct reconstruction may lead to poor performance. Our proposed Image Patch Supplement algorithm can supplement the missing information, as the experiment shows, an average of 4.1% mIoU can be improved. The Pascal VOC2012 dataset (224 crop size, 20 classes) and the Cityscape dataset (448 crop size, 19 classes) are used in the comparative experiments. With the Mask Ratio setting to 50%, in terms of the prediction region, the proposed model achieves 91.0% and 86.4% of mIoU on Pascal VOC 2012 and Cityscape, respectively, outperforming other current supervised semantic segmentation models. Our code and models are available at <https://github.com/jjrccop/Label-Mask-Auto-Encoder>*

## 1. Introduction

As a pixel-level classification task, semantic segmentation [19, 34] is sensitive to annotation integrity and precision, which may affect the model's overall performance. The conventional semi-supervised semantic segmentation model is based on the end-to-end framework where the student model continuously learns the pseudo-labels [45] generated by the teacher model [18, 29, 36]. As the model is

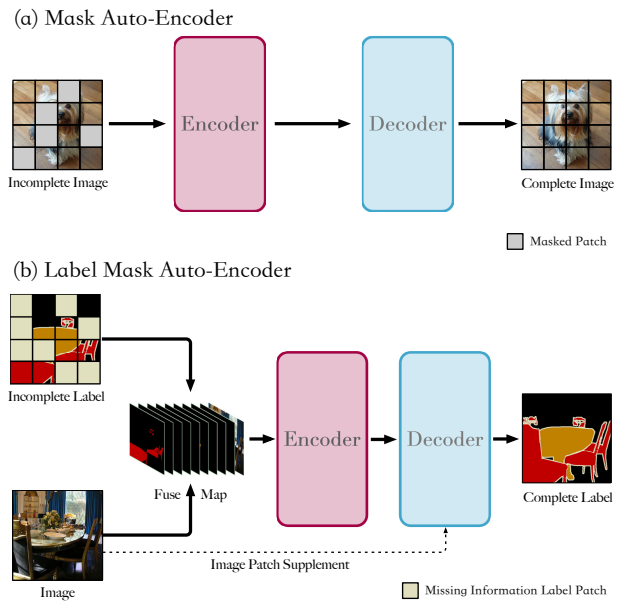


Figure 1. **An illustration between the MAE and our main idea.**  
 (a) MAE conduct a cover and reconstruct strategy on image information, which can learn a feature to complete the incomplete image.  
 (b) To refine the pixel-level on the label of the semantic segmentation dataset, we propose a Label Mask AutoEncoder framework. To fully use the input firstly, we present a strategy to fuse the Incomplete Label and the corresponding Image, namely Stack Fusion, to get the Fuse Map. Secondly, we perform the cover-reconstruct pipeline to get the final accurate prediction. For detail, we design a Image Patch Supplement algorithm to supplement the image information during the pipeline, which can be improved an average of 4.1% mIoU.

constantly updated, the quality of the pseudo-labels will continue to improve, thereby realizing the expansion of the dataset. Since the semantic segmentation dataset annotation, which requires professional knowledge, is usually labor-intensive and time-consuming, it may lead to the problem of un-integrity or imprecise labeling.

Inspired by Mask AutoEncoder(MAE)'s [16] cover and

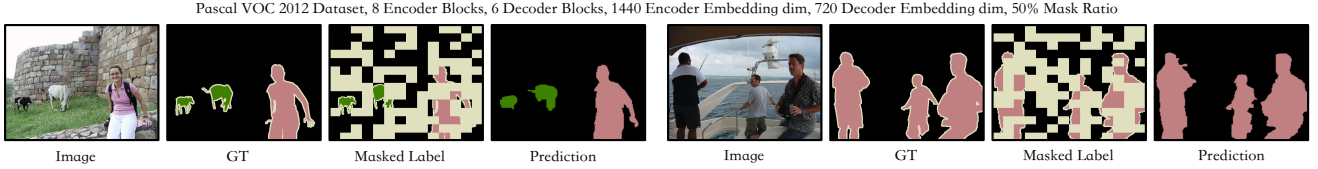


Figure 2. **The performance of the Label Mask AutoEncoder.** “Masked Label” denotes the complete label after randomly mask, as the “Prediction” shown, the follow up cover-reconstruct pipeline will complete the masked area.

reconstruct strategy, we propose the **Label Mask AutoEncoder**(L-MAE) method, which only needs to input an incomplete label information and the corresponding image, and then the detailed label of the image can be predicted. As shown in Fig. 1, generally, the proposed L-MAE process the label-image pair using the **Stack Fusion** strategy to achieve a better fusion effect. In detail, the label is separated into the *class\_number* dimension(s), and the 3 image layers (RGB) are concatenated to the rear of it to get the Fuse Map that would be used for the following pipeline. Our L-MAE has the following two characteristics: 1) Compared with supervised models [3, 27, 31], considering the need to enhance the existing label data, the input data of the proposed model is the pair of image and label, instead of the simple image information; 2) Compared with conventional semi-supervised models, our propose L-MAE adopts the covering and reconstructing pipeline instead of the Mean-Student model.

In the inference stage, as shown in Fig. 1(b), the data input into the network are image-label pairs. The Mask Selector algorithm is used to find the patches, i.e., areas of the higher proportion of the background in a specific label, then cover and reconstruct these patches with the L-MAE, which is trained by the same data distribution [9, 46], to obtain a supplementary label. The masked information may overflow into the solution space during the training process, so that a set of mask patch numbers are randomly generated first, then all the pixels of the patch are set to 255 to get the masked label. The image and masked label input into the model are fused using the Stack Fusion strategy, and then Patch Embedding is performed to obtain the Fuse Map Patch. Then discard the corresponding patch according to the previous mask patch number, and use the encoder module to extract the information that needs attention [35] to obtain the Feature Patch. Moreover, insert the Image Patch into the corresponding position of the Feature Patch according to the mask patch number. Finally, input all the information into the decoder module to get the sufficient label.

For the experimental process, we used the Pascal VOC 2012 dataset and the Cityscape dataset [9] to test the performance of L-MAE. Furthermore, ablation experiments are set for the number of Encoder-Decoder blocks, Encoder-Decoder Embedding Dimension, Mask Ratio, and the Image Patch Supplement algorithm. In order to equally mea-

sure the performance gap between L-MAE and other supervised semantic segmentation models, a new mIoU-based measurement metric that only focus on the mIoU of the reconstructed area is designed, namely Predict Area mean Intersection overUnion (PA-mIoU). The experimental results show that the performance of the proposed model achieves 91.0% and 86.4% of PA-mIoU on the dataset of Pascal VOC 2012 and Cityscape, respectively, when the mask ratio is set to 50%. Likewise, it reaches 89.2% and 85.8% of PA-mIoU on the dataset of Pascal VOC 2012 and Cityscape, respectively, when the mask ratio is set to 60%. In summary, the proposed model outperforms existing conventional semantic segmentation models, and our contributions are three-fold:

- We propose a Label Mask AutoEncoder(**L-MAE**) with a Stack Fusion module for the present task, which is different from the conventional semi-supervised semantic segmentation solves, is to complete the pixel-level information in a specific label.
- We design a Image Patch Supplement(IPS) algorithm to implement the semantic segmentation dataset on the Mask AutoEncoder framework. The IPS takes into account the sementic segmentation dataset characteristics, which improves the performance of the cover-reconstruct pipeline.
- We present a new measurement metric **Predict Area mean overUnion**(PA-mIoU), to fairly evaluate the capability of the L-MAE with other conventional models. Experimental results demonstrate that the proposed **L-MAE** can achieve **SOTA** performance compared with traditional solutions, which proves the effectiveness and superiority of the proposed method.

## 2. Related Work

### 2.1. Vision Transformer and MAE

Vision Transformer(ViT) [12], as the first pure Transformer model for image classification, directly splits an image into nonoverlapping fixed-size patches, adds position embedding, and feeds them to a standard Transformer. It achieves an impressive trade-off between speed and accuracy compared to convolutional neural networks on image

classification tasks and solves a problem that has plagued Computer Vision for a long time, how to transmit the image as input into the Transformer and retain the position information of the image. As the model and dataset size grows, there is still no sign of performance saturation. Although ViT works well for image classification, it requires large-scale annotated datasets. Inspired by the application of self-supervised models in NLP, such as BERT [10], MAE was proposed by He et al. as a self-supervised learning method [1, 11] for the training of computer vision models. Self-supervised learning mainly uses auxiliary tasks (pretext) to mine its own supervision information from large-scale unsupervised data and trains the network through the constructed supervision information so that it can learn valuable representations for downstream tasks and reduces reliance on large-scale annotated data. MAE proposed an asymmetric encoder-decoder architecture in which the encoder operates only on a subset of visible patches (tokens without masks). Then, there is a lightweight decoder that reconstructs the original image from the latent representation and mask tokens. As a result, the authors found that masking a high proportion of input image patches (e.g. 75%) turns into a meaningful self-supervised task. Combining these two designs enables efficient training of large models: their models train faster (by 3 $\times$  or more) and effectively improve the accuracy.

## 2.2. SegNeXt

Semantic segmentation is a fundamental computer vision task. In recent years, a large number of models have been proposed to try to achieve better performance on some basic semantic segmentation datasets. Transformer-based models dominate the field of semantic segmentation due to the efficiency of self-attention in encoding spatial information, but they usually have a large overhead in time and memory. Therefore, Guo et al. proposed SegNeXt [15], a simple convolutional network architecture for semantic segmentation. Its encoder module employs convolutions that introduce multi-scale convolutional attention and shows that convolutional attention is a more efficient way to encode contextual information than the self-attention mechanism in Transformer. Compared with the Transformer-based self-attention model, the model has better performance and lower overhead.

## 2.3. U2PL

The traditional semi-supervised semantic segmentation model is based on an end-to-end framework. The student model continuously learns the pseudo-labels generated by the teacher model. As the model is constantly updated, the quality of the pseudo-labels will continue to improve, thereby realizing the expansion of the dataset. Wang et al. [36] propose an efficient pipeline to fully utilize unlabeled

data, which separates reliable and unreliable pixels via the entropy of predictions, pushes each unreliable pixel to a category-wise queue that consists of negative samples, and manages to train the model with all candidate pixels. Ultimately, their model achieves SOTA performance on multiple semi-supervised semantic segmentation datasets. Since semantic segmentation dataset annotation requires higher labor costs and more time costs, especially in the professional field [23, 32]. While semi-supervised methods usually use only a small fraction of labeled datasets, they can approach the accuracy of supervised methods. Unlike traditional semi-supervised models trained on part labeled data and part unlabeled data, our model is trained using only incompletely labeled labels. Finally, our model achieves higher accuracy than supervised models in incompletely annotated regions.

## 3. Label Mask AutoEncoder

Although the Label corresponding to the Image can also be calculated using the traditional semantic segmentation model, this calculation method cannot fully use the existing data when some regions in the data have been marked. The Label MAE proposed by us can use the data of the labeled area in the Label, combined with the Image information, to calculate the Label information of the unlabeled area.

In this section, we illustrate the component of our Label MAE. It has three core designs to make it suitable for completing the label, namely Label Extend, Asymmetric Encoder-Decoder and Image Residual Connect. The details will be illustrated in the following.

### 3.1. Stack Fusion

We have tried a variety of methods [4, 22] for how to fuse the existing Label and Image: the first is to attach the single-channel Label information directly to the RGB 3-channel Image information in the form of concat. However, in practice, we found that after the subsequent tasks were performed, the results were consistent with the performance of the supervised semantic segmentation model [8, 24, 37]; the existing Label information was not captured. After the first failure, we thought that the Label information might be submerged in the Image information, and the fusion method was designed again. We copied the single-channel Label information three times and inserted it after each RGB channel separately. But the improvement was slight. Finally, we rethought the structure of the semantic segmentation model itself: the network’s final output is often a vector of class number dimension, which is not the same as the original Label information dimension. The previous methods may cause the Label information input to the network to be underutilized. Based on this feature, we finally tried to expand the Label into the class number dimension, concat the image information, and then sent it to the subsequent Encoder-

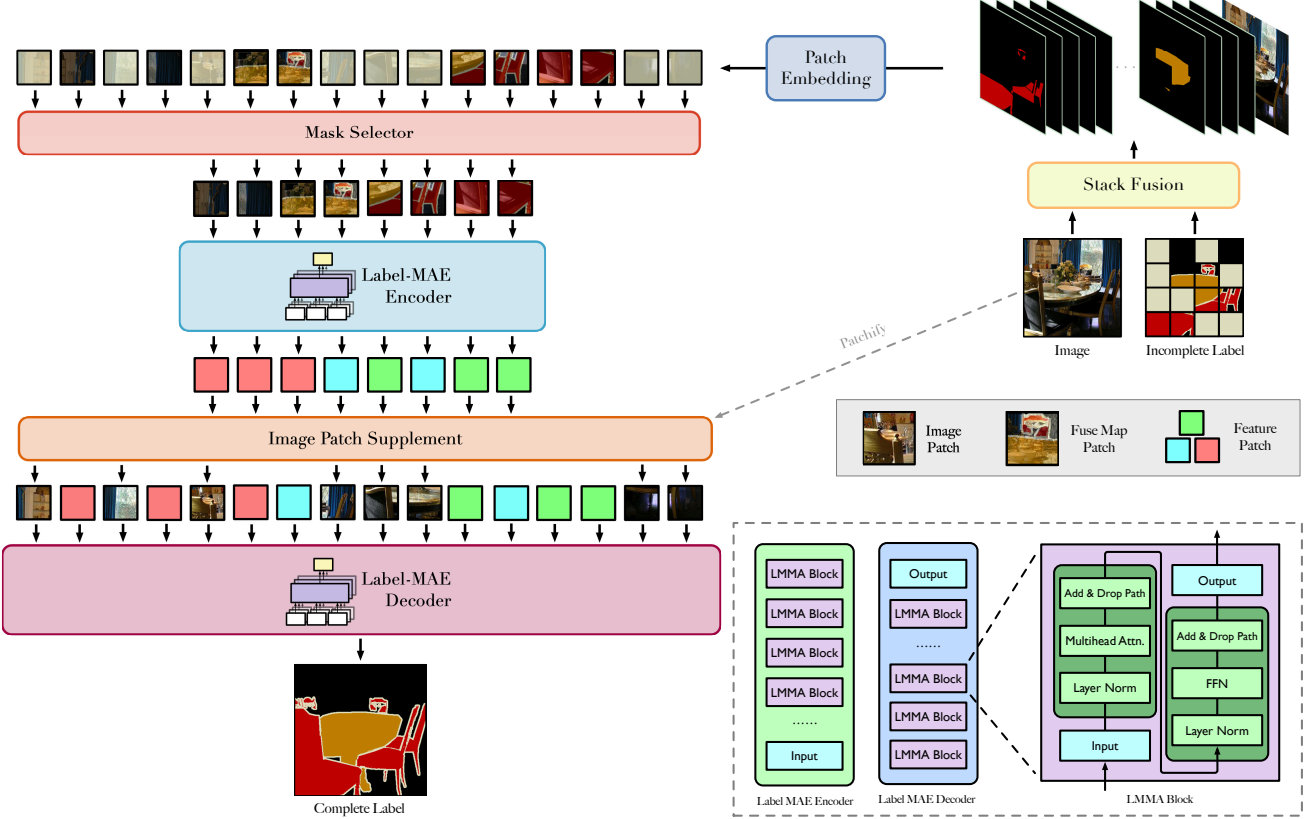


Figure 3. **The overview of the proposed Label Mask AutoEncoder(L-MAE) framework.** L-MAE mainly consists of a Stack Fuse module, a Mask Selector, an L-MAE Encoder, an L-MAE Decoder, and an Image Patch Supplement module. The L-MAE Encoder is applied to the small subset of visible fuse map patches, while the L-MAE Decoder is applied to the masked part. The Image Patch Supplement is used to supplement the image patch to the masked position, the image information here which has lost after performing the Mask Selector module.

Decoder. We obtained a performance that exceeded the current SOTA (only for the prediction area).

In detail, for the Label  $L \in \mathbb{R}^{H \times W \times 1}$  input to the network, we separately extract every category's label, to form a stack of separate Label images, and concatenate them with original Image  $I \in \mathbb{R}^{H \times W \times 3}$  as the final Fuse Map  $F \in \mathbb{R}^{H \times W \times (N+3)}$ , where the  $N$  here is class number. The progress can be described as follow,  $l_i (i = 1, 2, \dots, N)$  is the  $i$ -th class label:

$$FuseMap = \text{Concat}(l_1, l_2, \dots, l_N, image) \quad (1)$$

Before the next step, the Fuse Map will first go through Patch Embedding [14]. According to the patch size  $p$ , the feature  $F_f \in \mathbb{R}^{L \times (N+3)}$  can be obtained first, where  $L = \frac{H \times W}{p \times p}$ . Then it will be linearly mapped [28] into  $F_f \in \mathbb{R}^{L \times \tilde{e}}$  and add position informational to it, where  $\tilde{e}$  is encoder embedding dimension, the process can be for-

mulated as follows:

$$PE(pos, 2i) = \sin(pos/10000^{2i/\tilde{e}}) \quad (2)$$

$$PE(pos, 2i + 1) = \cos(pos/10000^{2i/\tilde{e}}) \quad (3)$$

where  $i$  indexes each patch, and  $pos$  is the position of each element of the input.

### 3.2. Mask Selector

Some information of  $F_f$  needs to be discarded in the training stage and inference stage, and then send  $F_f$  to the subsequent encoder and decoder. Different discarding strategies are used for different stages.

**Training Phase.** In order to enable the network to learn the function that can complete the Label, we randomly discard a part of patches in  $F_f$ . The number of discarded patches is  $l = \lfloor L \times m \rfloor$  where  $m$  is mask ratio.

**Inference Phase.** During the inference phase, the patches with a large area of background should be discarded and then reconstruct them. To achieve this function, the proportion of background for each patch is calculated, and then

we only to discard the top  $l$  patches where  $l = \lfloor L \times m \rfloor$ . In this way, we can avoid discarding patches with important information, and only focus on areas with large background. In practice, different mask ratios can be set to train the model to adapt to different situations.

### 3.3. Label MAE Encoder & Decoder

Our proposed L-MAE model uses the asymmetrical Encoder-Decoder architecture. The encoder is responsible for processing the rest patches, while the decoder process features from all patches.

**Image Patch Supplement.** We consider that if the Fuse Map is directly discarded at the patch level, the label information contained in these patches may be lost. So unlike MAE, which uses a normal distribution [20] for padding, we first used Patch Embedding that maps each patch into a vector  $F_{di} \in \mathbb{R}^{L \times \tilde{d}}$ , where  $\tilde{d}$  is decoder embedding dimension, and found the patch with the corresponding number on  $F_{di}$  according to the discarded patch number recorded before, finally inserted these patches into the  $F_e \in \mathbb{R}^{(L-l) \times \tilde{d}}$  output from the Encoder. We name this method Image Patch Supplement. Experiments have shown that the mIoU of the prediction area is significantly increased after using this method.

**Encoder & Decoder.** The Encoder uses N (The default setting is 12) LMMA Blocks, and the Decoder uses M (The default setting is 8) LMMA Blocks. For the encoder input  $x \in \mathbb{R}^{(L-l) \times \tilde{e}}$ , and decoder input  $x \in \mathbb{R}^{L \times \tilde{d}}$ . The formula of LMMA Block is as follows:

$$LMMABlock_1 = x + DropPath(MulAttn(x)) \quad (4)$$

$$LMMABlock_2 = x + DropPath(FFN(x)) \quad (5)$$

The Multi-Head Attention (MulAttn) module can perform multiple sets of self-attention processing on the original input sequence, then splicing the results of each set of self-attention to perform a linear transformation to obtain the final output result. Each group of self-attention is a Single-Head Attention. The first step will randomly initialize three vectors,  $W^Q, W^K, W^V$ . The  $Q, K, V$  can be calculated by:

$$Q_i = W_i^Q X, K_i = W_i^K X, V_i = W_i^V X \quad (6)$$

$Q, K$ , and  $V$  in the above formula are Query, Key, and Value, respectively. The input data  $x$  will use  $Q$  to retrieve the similar parts of the  $K$  by multiplication, the correlation coefficient will be calculated through softmax, and finally, the  $V$  will be calculated. By weighted summation, an output vector can be obtained, and the formula is as follows:

$$Z_i = softmax\left(\frac{Q_i K_i^T}{\sqrt{d_k}}\right) V_i \quad (7)$$

$$MulAttn(Q, K, V) = concat(Z_1, \dots, Z_h) W^O \quad (8)$$

where  $h$  represents the number of heads,  $W^O \in \mathbb{R}^{hd_v \times d_{model}}$ ,  $W^Q \in \mathbb{R}^{d_{model} \times d_k}$ ,  $W^K \in \mathbb{R}^{d_{model} \times d_k}$  and  $W^V \in \mathbb{R}^{d_{model} \times d_v}$  are projected parameter matrices.  $Z_i$  is the output vector of each. In original Transformer, they employ  $h = 8$  parallel attention layers and for each heads they use  $d_k = d_v = d_{model}/h = 64$ . Although there are many heads in the multi-head attention mechanism, the final complexity is similar to that of single-head attention.

A Feed-Forward Neural networks(FFN) are applied to the encoder and decoder in the last part, followed by a layer normalization [2]. FFN are calculated as follows:

$$FFN(x) = RELU(W_1 x + b_1) W_2 + b_2 \quad (9)$$

Although the same linear transformation is used for different positions, different parameters are used in feed-forward networks from one layer to another.

### 3.4. Loss Design

For the pipeline generated label  $x$  and the given original label  $y$ , a cross entropy loss [30] is adopted to optimize the relationship between two modalities, where  $x$  is encouraged to be similar with its corresponding  $y$  and dissimilar with other irrelatvant  $y$ . For detail, to solve the problem of performance degradation caused by the different proportions of each category in the segmentation task, we designed a weight calculation algorithm, so that each category can calculate the loss more balanced according to the proportion in the dataset. For the input  $x$  and  $y$ , the whole loss calculate process can be formulated as:

$$w_i = 1 - 1/(1 + \beta \cdot \exp(-\frac{x_i - E(x)}{V(x) + \xi}))^\gamma \quad (10)$$

$$l_n = -w_i \cdot \log \frac{\exp(x_{n,y_n})}{\sum_{i=1}^C \exp(x_{n,i})} \cdot 1\{y_n \neq \hat{y}_n\} \quad (11)$$

$$\ell(x, y) = \sum_{i=1}^{\mathcal{N}+1} l_i \cdot \frac{1}{\sum_{n=1}^{\mathcal{N}+1} w_{y_n} \cdot 1\{y_n \neq \hat{y}_n\}} \quad (12)$$

Where  $i \in \mathcal{N}$ ,  $\hat{y}_n$  is the ignore index,  $\ell$  is the loss function. For detail,  $\beta$  and  $\gamma$  are the learnable bias,  $\mathcal{N}$  means the number of class, which the  $\mathcal{N} + 1$  is also the output vector dimension,  $x_n$  and  $y_n$  here is the dimension  $n$  of the prediction  $x$  and the real label  $y$ ,  $w_{y_n}$  means for the dimension  $n$ , the loss weight of class  $y_n$ , ignore index  $\hat{y}_n$  is the background class, which not take account in the loss calculation.

## 4. Experiment

In this section, we introduce the technical details of applying our proposed Label MAE first. Then we design and conduct comparative experiments on Pascal VOC 2012 and Cityscape datasets to compare the performance differences

Table 1. Comparison with the super-vised sementic segmentation state-of-the-art approach on Pascal VOC 2012 and Cityscape dataset. For fairly, **our results use the PA-mIoU metric**. “m” denotes the Mask Ratio, while our L-MAE choose the hyper-parameter combination of Encoder Block is 8, Decoder Block is 6, Encoder Embedding Dimension is 1440, and Decoder Embedding Dimension is 720.

Methods	aero	bike	bird	boat	bottle	bus	car	cat	chair	cow	table	dog	horse	mbike	person	plant	sheep	sofa	train	tv	mIoU
RefineNet [26]	95.0	73.2	93.5	78.1	84.8	95.6	89.8	94.1	43.7	92.0	77.2	90.8	93.4	88.6	88.1	70.1	92.9	64.3	87.7	78.8	84.2
ResNet38 [17]	96.2	75.2	95.4	74.4	81.7	93.7	89.9	92.5	48.2	92.0	79.9	90.1	95.5	91.8	91.2	73.0	90.5	65.4	88.7	80.6	84.9
PSPNet [44]	95.8	72.7	95.0	78.9	84.4	94.7	92.0	95.7	43.1	91.0	80.3	91.3	96.3	92.3	90.1	71.5	94.4	66.9	88.8	82.0	85.4
Deeplabv3 [5]	96.4	76.6	92.7	77.8	87.6	96.7	90.2	95.4	47.5	93.4	76.3	91.4	97.2	91.0	92.1	71.3	90.9	68.9	90.8	79.3	85.7
EncNet [42]	95.3	76.9	94.2	80.2	85.3	96.5	90.8	96.3	47.9	93.9	80.0	92.4	96.6	90.5	91.5	70.9	93.6	66.5	87.7	80.8	85.9
DFN [38]	96.4	78.6	95.5	79.1	86.4	97.1	91.4	95.0	47.7	92.9	77.2	91.0	96.7	92.2	91.7	76.5	93.1	64.4	88.3	81.2	86.2
SDN [13]	96.9	78.6	96.0	79.6	84.1	97.1	91.9	96.6	48.5	94.3	78.9	93.6	95.5	92.1	91.1	75.0	93.8	64.8	89.0	84.6	86.6
Deeplabv3+ [6]	97.0	77.1	97.1	79.3	89.3	97.4	93.2	96.6	56.9	95.0	79.2	93.1	97.0	94.0	92.8	71.3	92.9	72.4	91.0	84.9	87.8
ExFuse [43]	96.8	80.3	97.0	82.5	87.8	96.3	92.6	96.4	53.3	94.3	78.4	94.1	94.9	91.6	92.3	81.7	94.8	70.3	90.1	83.8	87.9
MSCI [25]	96.8	76.8	97.0	80.6	89.3	97.4	93.8	97.1	56.7	94.3	78.3	93.5	97.1	94.0	92.8	72.3	92.6	73.6	90.8	85.4	88.0
MRFM [39]	<b>97.1</b>	78.6	<b>97.1</b>	80.6	89.7	<b>97.3</b>	<b>93.6</b>	<b>96.7</b>	59.0	<b>95.4</b>	81.1	93.2	<b>97.5</b>	<b>94.2</b>	<b>92.9</b>	72.3	93.1	74.2	91.0	85.0	88.4
L-MAE w/ m=0.6	89.5	58.8	92.3	86.4	91.3	94.9	89.6	95.3	79.1	93.7	89.6	93.4	91.0	90.5	89.4	85.6	96.1	93.0	96.0	87.5	<b>89.1</b>
L-MAE w/ m=0.5	89.9	64.5	91.4	<b>89.2</b>	<b>92.1</b>	95.9	90.6	96.4	<b>82.1</b>	94.6	<b>91.2</b>	<b>94.7</b>	94.3	92.4	91.1	<b>87.8</b>	<b>97.8</b>	<b>94.0</b>	<b>96.5</b>	<b>93.4</b>	<b>91.0</b>

Methods	road	swalk	build.	wall	fence	pole	tlight	tsign	veg.	terrain	sky	person	rider	car	truck	bus	train	mcycle	bicycle	mIoU
VPLR [47]	98.8	87.8	94.2	64.1	65.0	72.4	79.0	82.8	94.2	74.0	96.1	88.2	75.4	96.5	78.8	94.0	91.6	73.7	79.0	83.5
HRNet-OCR [40]	98.8	88.3	94.1	66.9	66.7	73.3	80.2	83.0	94.2	74.1	96.0	88.5	75.8	96.5	78.5	91.8	90.1	73.4	79.3	83.7
P-DeepLab [7]	98.8	88.1	94.5	68.1	68.1	74.5	80.5	83.5	94.2	74.4	96.1	89.2	77.1	96.5	78.9	91.8	89.1	76.4	79.3	84.2
iFLYTEK-CV	98.8	88.4	94.4	68.9	66.8	73.0	79.7	83.3	94.3	74.3	96.0	88.8	76.3	96.6	84.0	<b>94.3</b>	91.7	74.7	79.3	84.4
SegFix [41]	98.8	88.3	94.3	67.9	67.8	73.5	80.6	83.9	94.3	74.4	96.0	89.2	75.8	<b>96.8</b>	83.6	94.1	91.2	74.0	80.0	84.5
HMSA [33]	<b>99.0</b>	89.2	94.9	71.6	69.1	75.8	<b>82.0</b>	<b>85.2</b>	94.5	75.0	<b>96.3</b>	<b>90.0</b>	79.4	96.9	79.8	94.0	85.8	77.4	81.4	85.1
L-MAE w/ m=0.6	97.4	89.1	94.1	89.2	90.7	74.8	66.0	71.7	93.9	88.6	94.5	81.7	73.8	93.6	89.6	89.8	90.3	79.3	78.0	<b>85.6</b>
L-MAE w/ m=0.5	98.0	<b>91.9</b>	<b>95.8</b>	<b>91.9</b>	<b>93.0</b>	<b>81.4</b>	74.4	78.6	<b>95.7</b>	<b>91.1</b>	95.8	86.2	<b>79.7</b>	95.3	<b>91.9</b>	91.7	<b>92.1</b>	<b>83.6</b>	<b>82.9</b>	<b>86.4</b>

between L-MAE and (semi-)supervised semantic segmentation models. Finally, we design a set of extensive ablation experiments to analyze the effect of Encoder Block, Decoder Block, Encoder Embedding Dimension, Decoder Embedding Dimension, and Mask Ratio on performance in Label MAE.

#### 4.1. Experiment Setup

Our L-MAE is built using the Pytorch framework and the Adam optimizer [21] with 0.9 of momentum, and weight decay is set to 0.0001. Further, the Reduce Learning Rate On Plateau strategy with min mode is used, which reduces the learning rate with a specified factor after a preset number of patient rounds, which is decided by threshold of loss dropping. In actual use, we set these parameters as follows: 5 of the patient rounds, 0.001 of the threshold, and 0.8 of the factor. The experiments were performed using Nvidia Tesla A40 for 400 epochs on Pascal VOC and Cityscape. On Pascal VOC, the Image and Label are randomly cropped to  $448 \times 448$ , and then scaled to  $224 \times 224$ , while in Cityscape which is randomly cropped to  $448 \times 448$ . During training, a batch size of 24 was used in Pascal VOC, and a batch size of 48 was used in Cityscape.

#### 4.2. PA-mIoU

It is unfair to use the general global area mIoU solely to other semantic segmentation models in the comparative experiment, which may lead to low efficient of measuring the network performance. So we designed a new evaluation metric: **Predict Area mean Intersection overUnion** (PA-mIoU), which will only focus on the mIoU in discarded

area. In the specific implementation, the number list  $i \in \mathbb{R}^l$  of the patch is discarded according to the Mask Selector, and a mask  $m \in \mathbb{R}^{H \times W}$  that can cover the entire label is produced. Then according to whether each position in the mask stores 0 or 1 (0 is the reserved area, 1 is the discarded area), to determine whether the result of the label in the corresponding position is counted.

#### 4.3. Comparative Experiments

In comparative experiments, we use several excellent supervised semantic segmentation models to compare with our Label Mask AutoEncoder. By comparing the PA-mIoU of L-MAE with the mIoU of other models, we found that as the Mask Ratio decreases, the PA-mIoU will continue to rise, and exceeds the existing state-of-the-art model when the Mask Ratio is 50%.

##### 4.3.1 Results on Pascal VOC 2012

Pascal VOC 2012 is an upgraded version of the Pascal VOC 2007 dataset, with a total number of 11530 images. For the segmentation task, the train/val of VOC2012 contains all images from 2007 to 2012, with 2913 images totaling, 2513 of which used as the training set and 400 images are used as the validation set. For the comparison with other general semantic segmentation models, when the mask ratio is set to 50%, our L-MAE can achieve **94.6%** Global mIoU, and **91.0%** PA-mIoU; when the mask ratio is set to 60%, our L-MAE can achieve **92.6%** mIoU, and **89.1%** PA-mIoU. As shown in the top of the Table 1, the proposed method outperforms the current conventional performance.

Table 2. Comparison between different hyper-parameter combinations. “EB” is Encoder Block, “DB” is Decoder Block, “ED” is Encoder Embedding Dimension, “DD” is Decoder Embedding Dimension. We also calculate the parameters(M) and the FLOPs(G) under various settings. Moreover, the calculation of the mIoU and the PA-mIoU include the background class.

EB	DB	ED	DD	#params.(M)	FLOPs(G)	mIoU	PA-mIoU
12	8	1024	512	186M	21G	94.1	90.5
		1440	720	362M	42G	94.1	90.4 ↓
8	6	1024	512	129M	15G	94.1	90.3
		1440	720	250M	29G	94.6 ↑	91.3 ↑
6	4	1024	512	98M	11G	94.2	90.4
		1440	720	188M	22G	94.6 ↑	91.2 ↑

### 4.3.2 Results on Cityscape

Cityscape dataset is collected from 50 cities in Germany and nearby countries, including street scenes in three seasons of spring, summer and autumn, with 5000 images of 27 cities with pixel-level semantic and instance annotation. For comparing, we set the Mask Ratio to 50% and 60%, respectively. As the result, our L-MAE can achieve **90.5%** Global mIoU, and **86.4%** PA-mIoU, when the Mask Ratio is 50%, while the **89.0%** Global mIoU, and **85.6%** PA-mIoU in 60% Mask Ratio. As shown in the bottom of the Table 1, L-MAE surpasses the legacy SOTA.

## 4.4 Ablation Study

To evaluate the impact and performance of each component in our model, we evaluate their effectiveness in this section. The Pascal VOC dataset(224 input size) is choosed to evaluate the model.

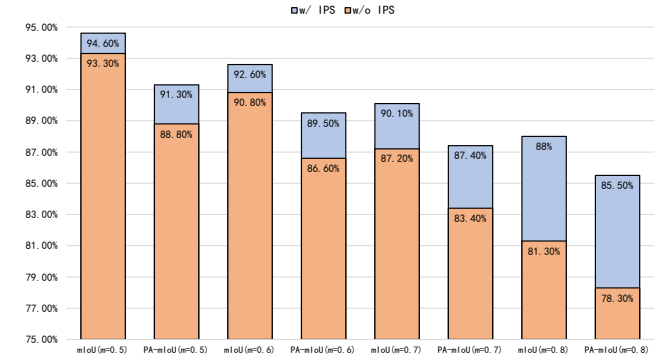
### 4.4.1 Parameter Setting Analysis

As shown in Table 2, we explore the performance of the L-MAE under different parameters. There are 4 main hyper-parameters for the network: encoder block number(EB), decoder block number(DB), encoder embedding dimension(ED), decoder embedding dimension(DD). We can find that when the block number is consistent, the performance will get worse as the embedding dimension fall. Nevertheless, expect for the case  $EB=12$ ,  $DB=8$ , when using  $ED=1440$  and  $DD=720$ , its PA-mIoU is lower than when  $ED=1024$  and  $DD=512$ . However, the global mIoU keeps the same, which means that the mIoU of the reserved area has risen. Based on the table results, we choose the combination of  $EB=8$ ,  $DB=6$ ,  $ED=1440$ , and  $DD=720$ .

### 4.4.2 Mask Ratio & Image Patch Supplement

We have explored the contribution of our Image Patch Supplement algorithm and the effect of Mask Ratio. As shown in Fig. 4, the mIoU average drop 3.0%, while the PA-mIoU

Figure 4. Ablation study on various Mask Ratio, and whether or not to use the Image Patch Supplement(IPS) algorithm. The calculation of the mIoU and the PA-mIoU include the background class. “m” means Mask Ratio.



average drop 4.1% after applying the Image Patch Supplement(IPS) algorithm. Meanwhile, we notice that the effect of IPS is different under various Mask Ratios. The higher the Mask Ratio, the more significant the improvement of PA-mIoU by IPS. Similarly, the use of IPS has different impacts on mIoU and PA-mIoU. For example, when the Mask Ratio=0.7, the decline of mIoU is smaller than that of PA-mIoU. The result demonstrates that the IPS is an essential algorithm to improve the accuracy, and it proves our IPS can supplement the image information to the property position of the model.

## 4.5 Qualitative Study

**Visualization.** As illustrated in Fig. 5, we present some visualization results with different setting, which demonstrates the benefits of each component in our proposed method. Firstly, under various Mask Ratio setting, compared with the L-MAE employed Image Patch Supplement, the model which without employing perform worse, because the cover process not only discard the label but the image, so the follow-up reconstruct can not use the image information at the masked position. Secondly, as the Mask Ratio raising, the model performance is not affected to much, which proves high stability of the model. Finally, our model can generate high-quality segmentation masks, which demonstrates the effectiveness of our proposed method, i.e., L-MAE.

**Failure Cases.** We visualize some insightful failed cases in Fig. 6. One type of failure is caused when predicting objects containing tubular structures. For the left example in Fig. 6, “green” is not enough to describe the region of the whole bicycle. Besides, for the right example, failures are also caused by the confusion of background information and masked areas in images. Obviously, the bottom right region is unrelated to “people”. Nevertheless, this issue

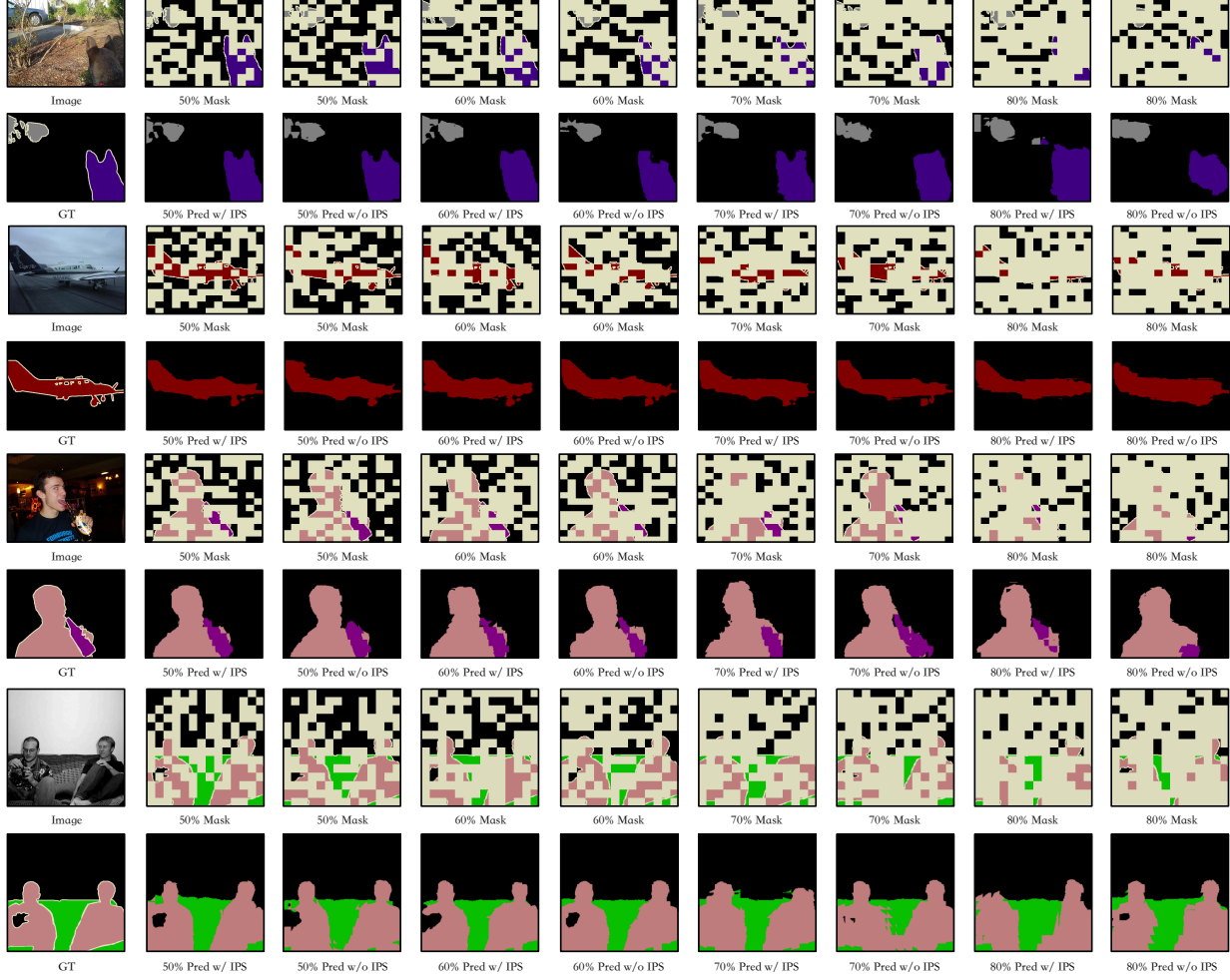


Figure 5. Qualitative examples with different settings.



Figure 6. Qualitative examples of failure cases.

can be alleviated by introducing other technologies, such as defining a specific class number for the mask part.

## 5. Conclusion

In this paper, we have investigated to leverage the power of Mask AutoEncoder (MAE) models to achieve pixel-level label complete. And, we have proposed an end-to-end Label Mask AutoEncoder (L-MAE) framework to well transfer the cover-reconstruct ability of the MAE model. Compared with the conventional methods, our proposed framework inherits the strong pixel rebuilding ability of the MAE, and the propose method can be used to reconstruct unknown

pixels with known label information. The designed Image Patch Supplement algorithm can supplement the image information at the desired location, and guarantees the integrity of information when performing completion tasks. Furthermore, the proposed Predict Area mean Intersection overUnion(PA-mIoU) can calculate the mIoU of the completion area, making the comparison between L-MAE and other traditional models fairer. We conduct comparative experiments on two commonly used datasets, along with extensive ablation studies to validate the effectiveness of each proposed component, and our approach significantly outperforms conventional methods without any pre-training.

## References

- [1] Dosovitskiy Alexey, Philipp Fischer, Jost Tobias, Martin Riedmiller Springenberg, and Thomas Brox. Discriminative unsupervised feature learning with exemplar convolutional neural networks. *IEEE Trans. Pattern Analysis and Machine Intelligence*, 99, 2015. 3
- [2] Jimmy Lei Ba, Jamie Ryan Kiros, and Geoffrey E Hinton. Layer normalization. *arXiv preprint arXiv:1607.06450*, 2016. 5
- [3] Vijay Badrinarayanan, Alex Kendall, and Roberto Cipolla. Segnet: A deep convolutional encoder-decoder architecture for image segmentation. *IEEE transactions on pattern analysis and machine intelligence*, 39(12):2481–2495, 2017. 2
- [4] Sean Bell, C Lawrence Zitnick, Kavita Bala, and Ross Girshick. Inside-outside net: Detecting objects in context with skip pooling and recurrent neural networks. In *Proceedings of the IEEE conference on computer vision and pattern recognition*, pages 2874–2883, 2016. 3
- [5] Liang-Chieh Chen, George Papandreou, Florian Schroff, and Hartwig Adam. Rethinking atrous convolution for semantic image segmentation. *arXiv preprint arXiv:1706.05587*, 2017. 6
- [6] Liang-Chieh Chen, Yukun Zhu, George Papandreou, Florian Schroff, and Hartwig Adam. Encoder-decoder with atrous separable convolution for semantic image segmentation. In *Proceedings of the European conference on computer vision (ECCV)*, pages 801–818, 2018. 6
- [7] Bowen Cheng, Maxwell D Collins, Yukun Zhu, Ting Liu, Thomas S Huang, Hartwig Adam, and Liang-Chieh Chen. Panoptic-deeplab: A simple, strong, and fast baseline for bottom-up panoptic segmentation. In *Proceedings of the IEEE/CVF conference on computer vision and pattern recognition*, pages 12475–12485, 2020. 6
- [8] Bowen Cheng, Ishan Misra, Alexander G Schwing, Alexander Kirillov, and Rohit Girdhar. Masked-attention mask transformer for universal image segmentation. In *Proceedings of the IEEE/CVF Conference on Computer Vision and Pattern Recognition*, pages 1290–1299, 2022. 3
- [9] Marius Cordts, Mohamed Omran, Sebastian Ramos, Timo Rehfeld, Markus Enzweiler, Rodrigo Benenson, Uwe Franke, Stefan Roth, and Bernt Schiele. The cityscapes dataset for semantic urban scene understanding. In *Proceedings of the IEEE conference on computer vision and pattern recognition*, pages 3213–3223, 2016. 2
- [10] Jacob Devlin, Ming-Wei Chang, Kenton Lee, and Kristina Toutanova. Bert: Pre-training of deep bidirectional transformers for language understanding. *arXiv preprint arXiv:1810.04805*, 2018. 3
- [11] Carl Doersch, Abhinav Gupta, and Alexei A Efros. Unsupervised visual representation learning by context prediction. In *Proceedings of the IEEE international conference on computer vision*, pages 1422–1430, 2015. 3
- [12] Alexey Dosovitskiy, Lucas Beyer, Alexander Kolesnikov, Dirk Weissenborn, Xiaohua Zhai, Thomas Unterthiner, Mostafa Dehghani, Matthias Minderer, Georg Heigold, Sylvain Gelly, et al. An image is worth 16x16 words: Trans-
- formers for image recognition at scale. *arXiv preprint arXiv:2010.11929*, 2020. 2
- [13] Jun Fu, Jing Liu, Yuhang Wang, Jin Zhou, Changyong Wang, and Hanqing Lu. Stacked deconvolutional network for semantic segmentation. *IEEE Transactions on Image Processing*, 2019. 6
- [14] Jonas Gehring, Michael Auli, David Grangier, Denis Yarats, and Yann N Dauphin. Convolutional sequence to sequence learning. In *International conference on machine learning*, pages 1243–1252. PMLR, 2017. 4
- [15] Meng-Hao Guo, Cheng-Ze Lu, Qibin Hou, Zhengning Liu, Ming-Ming Cheng, and Shi-Min Hu. Segnext: Rethinking convolutional attention design for semantic segmentation. *arXiv preprint arXiv:2209.08575*, 2022. 3
- [16] Kaiming He, Xinlei Chen, Saining Xie, Yanghao Li, Piotr Dollár, and Ross Girshick. Masked autoencoders are scalable vision learners. In *Proceedings of the IEEE/CVF Conference on Computer Vision and Pattern Recognition*, pages 16000–16009, 2022. 1
- [17] Kaiming He, Xiangyu Zhang, Shaoqing Ren, and Jian Sun. Deep residual learning for image recognition. In *Proceedings of the IEEE conference on computer vision and pattern recognition*, pages 770–778, 2016. 6
- [18] Ruifei He, Jihan Yang, and Xiaojuan Qi. Re-distributing biased pseudo labels for semi-supervised semantic segmentation: A baseline investigation. In *Proceedings of the IEEE/CVF International Conference on Computer Vision*, pages 6930–6940, 2021. 1
- [19] Wei-Chih Hung, Yi-Hsuan Tsai, Yan-Ting Liou, Yen-Yu Lin, and Ming-Hsuan Yang. Adversarial learning for semi-supervised semantic segmentation. *arXiv preprint arXiv:1802.07934*, 2018. 1
- [20] Mikhail Khodak, Neil Tenenholz, Lester Mackey, and Nicolo Fusi. Initialization and regularization of factorized neural layers. *arXiv preprint arXiv:2105.01029*, 2021. 5
- [21] Diederik P Kingma and Jimmy Ba. Adam: A method for stochastic optimization. *arXiv preprint arXiv:1412.6980*, 2014. 6
- [22] Tao Kong, Anbang Yao, Yurong Chen, and Fuchun Sun. Hypernet: Towards accurate region proposal generation and joint object detection. In *Proceedings of the IEEE conference on computer vision and pattern recognition*, pages 845–853, 2016. 3
- [23] Dmitrii Lachinov, Philipp Seeböck, Julia Mai, Felix Goldbach, Ursula Schmidt-Erfurth, and Hrvoje Bogunovic. Projective skip-connections for segmentation along a subset of dimensions in retinal oct. In *International Conference on Medical Image Computing and Computer-Assisted Intervention*, pages 431–441. Springer, 2021. 3
- [24] Feng Li, Hao Zhang, Shilong Liu, Lei Zhang, Lionel M Ni, Heung-Yeung Shum, et al. Mask dino: Towards a unified transformer-based framework for object detection and segmentation. *arXiv preprint arXiv:2206.02777*, 2022. 3
- [25] Di Lin, Yuanfeng Ji, Dani Lischinski, Daniel Cohen-Or, and Hui Huang. Multi-scale context intertwining for semantic segmentation. In *Proceedings of the European Conference on Computer Vision (ECCV)*, pages 603–619, 2018. 6

[26] Guosheng Lin, Anton Milan, Chunhua Shen, and Ian Reid. Refinenet: Multi-path refinement networks for high-resolution semantic segmentation. In *Proceedings of the IEEE conference on computer vision and pattern recognition*, pages 1925–1934, 2017. 6

[27] Jonathan Long, Evan Shelhamer, and Trevor Darrell. Fully convolutional networks for semantic segmentation. In *Proceedings of the IEEE conference on computer vision and pattern recognition*, pages 3431–3440, 2015. 2

[28] Bethany Lusch, J Nathan Kutz, and Steven L Brunton. Deep learning for universal linear embeddings of nonlinear dynamics. *Nature communications*, 9(1):1–10, 2018. 4

[29] Hieu Pham, Zihang Dai, Qizhe Xie, and Quoc V Le. Meta pseudo labels. In *Proceedings of the IEEE/CVF Conference on Computer Vision and Pattern Recognition*, pages 11557–11568, 2021. 1

[30] Gorkem Polat, Ilkay Ergenc, Haluk Tarik Kani, Yesim Ozen Alahdab, Ozlen Atug, and Alptekin Temizel. Class distance weighted cross-entropy loss for ulcerative colitis severity estimation. *arXiv preprint arXiv:2202.05167*, 2022. 5

[31] Olaf Ronneberger, Philipp Fischer, and Thomas Brox. U-net: Convolutional networks for biomedical image segmentation. In *International Conference on Medical image computing and computer-assisted intervention*, pages 234–241. Springer, 2015. 2

[32] Youyi Song, Lequan Yu, Baiying Lei, Kup-Sze Choi, and Jing Qin. Selective learning from external data for ct image segmentation. In *International Conference on Medical Image Computing and Computer-Assisted Intervention*, pages 420–430. Springer, 2021. 3

[33] Andrew Tao, Karan Sapra, and Bryan Catanzaro. Hierarchical multi-scale attention for semantic segmentation. *arXiv preprint arXiv:2005.10821*, 2020. 6

[34] Antti Tarvainen and Harri Valpola. Mean teachers are better role models: Weight-averaged consistency targets improve semi-supervised deep learning results. *Advances in neural information processing systems*, 30, 2017. 1

[35] Ashish Vaswani, Noam Shazeer, Niki Parmar, Jakob Uszkoreit, Llion Jones, Aidan N Gomez, Łukasz Kaiser, and Illia Polosukhin. Attention is all you need. *Advances in neural information processing systems*, 30, 2017. 2

[36] Yuchao Wang, Haochen Wang, Yujun Shen, Jingjing Fei, Wei Li, Guoqiang Jin, Liwei Wu, Rui Zhao, and Xinyi Le. Semi-supervised semantic segmentation using unreliable pseudo-labels. In *Proceedings of the IEEE/CVF Conference on Computer Vision and Pattern Recognition*, pages 4248–4257, 2022. 1, 3

[37] Enze Xie, Wenhui Wang, Zhiding Yu, Anima Anandkumar, Jose M Alvarez, and Ping Luo. Segformer: Simple and efficient design for semantic segmentation with transformers. *Advances in Neural Information Processing Systems*, 34:12077–12090, 2021. 3

[38] Changqian Yu, Jingbo Wang, Chao Peng, Changxin Gao, Gang Yu, and Nong Sang. Learning a discriminative feature network for semantic segmentation. In *Proceedings of the IEEE conference on computer vision and pattern recognition*, pages 1857–1866, 2018. 6

[39] Jianlong Yuan, Zelu Deng, Shu Wang, and Zhenbo Luo. Multi receptive field network for semantic segmentation. In *2020 IEEE Winter Conference on Applications of Computer Vision (WACV)*, pages 1883–1892. IEEE, 2020. 6

[40] Yuhui Yuan, Xilin Chen, and Jingdong Wang. Object-contextual representations for semantic segmentation. In *European conference on computer vision*, pages 173–190. Springer, 2020. 6

[41] Yuhui Yuan, Jingyi Xie, Xilin Chen, and Jingdong Wang. Segfix: Model-agnostic boundary refinement for segmentation. In *European Conference on Computer Vision*, pages 489–506. Springer, 2020. 6

[42] Hang Zhang, Kristin Dana, Jianping Shi, Zhongyue Zhang, Xiaogang Wang, Ambrish Tyagi, and Amit Agrawal. Context encoding for semantic segmentation. In *Proceedings of the IEEE conference on Computer Vision and Pattern Recognition*, pages 7151–7160, 2018. 6

[43] Zhenli Zhang, Xiangyu Zhang, Chao Peng, Xiangyang Xue, and Jian Sun. Exfuse: Enhancing feature fusion for semantic segmentation. In *Proceedings of the European conference on computer vision (ECCV)*, pages 269–284, 2018. 6

[44] Hengshuang Zhao, Jianping Shi, Xiaojuan Qi, Xiaogang Wang, and Jiaya Jia. Pyramid scene parsing network. In *Proceedings of the IEEE conference on computer vision and pattern recognition*, pages 2881–2890, 2017. 6

[45] Zhedong Zheng and Yi Yang. Rectifying pseudo label learning via uncertainty estimation for domain adaptive semantic segmentation. *International Journal of Computer Vision*, 129(4):1106–1120, 2021. 1

[46] Bolei Zhou, Hang Zhao, Xavier Puig, Tete Xiao, Sanja Fidler, Adela Barriuso, and Antonio Torralba. Semantic understanding of scenes through the ade20k dataset. *International Journal of Computer Vision*, 127(3):302–321, 2019. 2

[47] Yi Zhu, Karan Sapra, Fitzsum A Reda, Kevin J Shih, Shawn Newsam, Andrew Tao, and Bryan Catanzaro. Improving semantic segmentation via video propagation and label relaxation. In *Proceedings of the IEEE/CVF Conference on Computer Vision and Pattern Recognition*, pages 8856–8865, 2019. 6